

Accepted Manuscript

Antibacterial activity of gelatin/copper (II)-exchanged montmorillonite films

Josefa F. Martucci, Roxana A. Ruseckaite

PII: S0268-005X(16)30623-3

DOI: [10.1016/j.foodhyd.2016.10.030](https://doi.org/10.1016/j.foodhyd.2016.10.030)

Reference: FOOHYD 3648

To appear in: *Food Hydrocolloids*

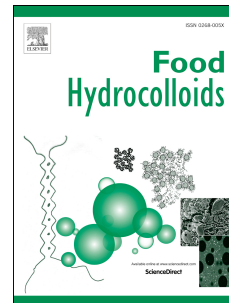
Received Date: 15 April 2016

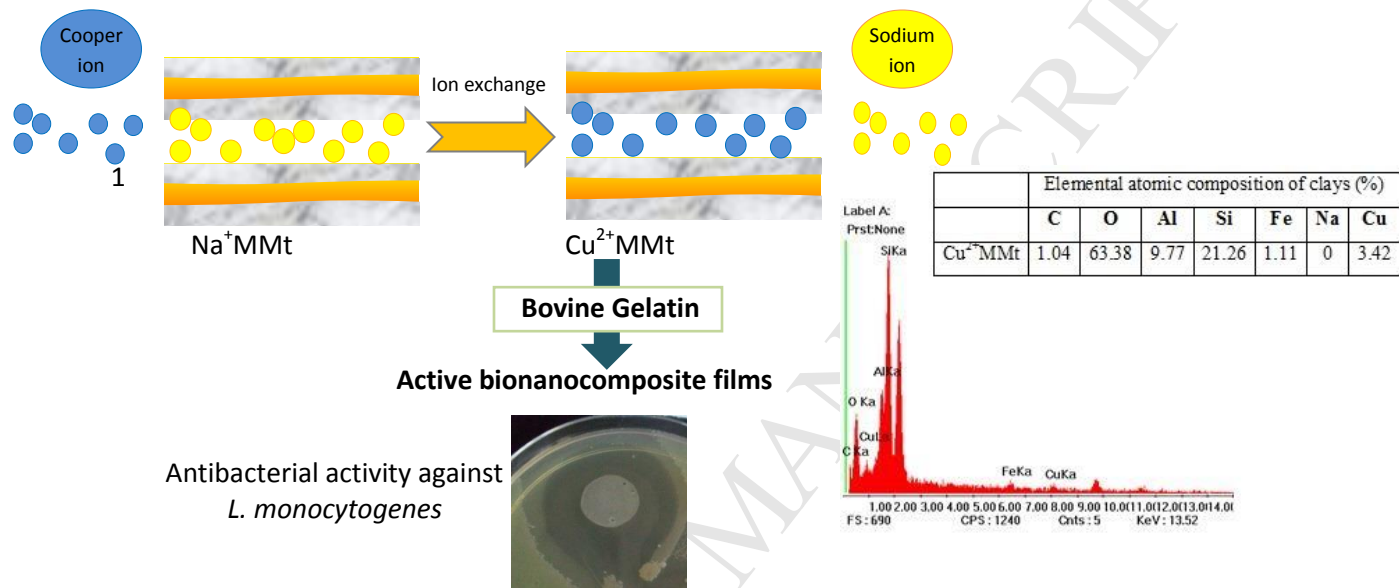
Revised Date: 18 October 2016

Accepted Date: 20 October 2016

Please cite this article as: Martucci, J.F., Ruseckaite, R.A., Antibacterial activity of gelatin/copper (II)-exchanged montmorillonite films, *Food Hydrocolloids* (2016), doi: 10.1016/j.foodhyd.2016.10.030.

This is a PDF file of an unedited manuscript that has been accepted for publication. As a service to our customers we are providing this early version of the manuscript. The manuscript will undergo copyediting, typesetting, and review of the resulting proof before it is published in its final form. Please note that during the production process errors may be discovered which could affect the content, and all legal disclaimers that apply to the journal pertain.





1 **Antibacterial activity of gelatin / copper (II)-exchanged montmorillonite films**

2

3

*Josefa F. Martucci & Roxana A. Ruseckaite**

4 Instituto de Investigaciones en Ciencia y Tecnología de Materiales (INTEMA),

5 Universidad Nacional de Mar del Plata – CONICET, Av. J.B.Justo 4302, B7608FDQ-

6 Mar del Plata, Argentina

7 *Corresponding author. E-mail: roxana@fi.mdp.edu.ar; rxane888@gmail.com

8

9

10

11

12

13

14

15

16

17

ABSTRACT

18 Cu (II) - exchanged montmorillonite (Cu^{2+}MMt) was prepared, characterized and
19 introduced into a bovine gelatin (Ge) matrix via a dissolution-intercalation method to
20 get antibacterial nanocomposite films. The maximum amount of exchanged cation did
21 not exceed the cation exchange capacity of the pristine montmorillonite (Na^+MMt), as
22 assessed by energy dispersive X-ray (EDX) spectroscopy. Cu^{2+}MMt showed
23 antibacterial activity *in vitro* against *Escherichia coli O157:H7* (Gram-negative) and
24 *Listeria monocytogenes* (Gram-positive) as revealed by the agar disc-diffusion assay.
25 The dispersion of clays in Ge films was monitored by X-ray diffraction (XRD) and
26 Scanning Electron Microscopy (SEM). Blending gelatin with 5 % w/w of clay increased
27 the tensile strength of the nanocomposite films in around 280 % while the elongation at
28 break and the water vapor permeability decreased in about 42 and 30 %, respectively,
29 regardless of the cation in clay. The Ge/ Cu^{2+}MMt film exhibited antibacterial
30 effectiveness against both pathogens tested under the same conditions, demonstrating a
31 stronger effect on *L. monocytogenes* than on *E. coli O157:H7*, since the cell wall of the
32 latter differs significantly and such difference could influence their vulnerability and
33 response to the active films. Therefore, the incorporation of low clay levels as a vehicle
34 for copper ions into gelatin matrix has demonstrated to be a good method for
35 developing functional materials that can be potentially applied to the design of food
36 contact items.

37

38 *Keywords: Bovine gelatin; Cupric ions; Montmorillonite; Nanocomposite; Active film;*
39 *Antimicrobial activity.*

40

41 **1. Introduction**

42 The inclusion of long-lasting biocide agents in natural polymer matrices is acting as a
43 driving force for the development of new environmentally sound packaging concepts
44 that extend shelf-life, while maintaining the food safety and quality of packed food
45 (Rhim et al. 2013).

46 Certain naturally occurring metal ions such as copper, silver, zinc, palladium, and
47 titanium, which, in some cases, are essential minerals, are active antimicrobials against
48 a very broad spectrum of bacteria, yeasts and fungi with no adverse effects on
49 eukaryotic cells (Llorens et al. 2012). CuSO_4 and $\text{Cu}(\text{OH})_2$ have been widely applied to
50 animal production as traditional inorganic antibacterial materials (Hu et al. 2005).
51 However, the direct inclusion of Cu^{2+} in polymer formulations has been limited by
52 uncontrolled leaching. One way to prevent early burst is by immobilizing Cu^{2+} ions onto
53 inorganic carriers, including zeolites (Drelich et al. 2011) and clay minerals (Mosser et
54 al. 1997; He et al. 2001; Zhou et al. 2004; Tong et al. 2005; Hu et al. 2005; Hu & Xia
55 2006). Montmorillonite (MMt) is a hydrophilic and highly water dispersible 2:1 layered
56 aluminium phyllosilicate with good adsorption ability, high cation - exchange capacity,
57 and drug-carrying capability (Xia et al. 2010) combined with other favorable features
58 such as high surface area and chemical inertness (Drelich et al. 2011). The negatively
59 charged interlayer regions of MMt are mainly filled with exchangeable positively
60 charged ions, such as Na^+ , K^+ , Ca^{2+} , etc., thus, active Cu^{2+} ions can be accommodated in
61 the interlayer space, providing materials with a long-lasting action period (He et al.
62 2001; Hu et al. 2005; Hu & Xia 2006). The immobilization of Cu^{2+} onto MMt, together
63 with its antimicrobial action, has been extensively documented (Mosser et al. 1997; He
64 et al. 2001; Zhou et al. 2004; Tong et al. 2005; Kloprogge et al. 2006; Hu et al. 2005;
65 Hu and Xia 2006; Malachovà et al. 2009, 2011; Pereira et al. 2013). Even so, scant

66 literature explores the antimicrobial activity of Cu^{2+} MMt-polymer nanocomposites.
67 Bruna and others (2012) developed low density polyethylene (LDPE)/ Cu^{2+} MMt films
68 and reported a reduction of 94 % of *Escherichia coli* O157:H7 colonies at 4 % w/w
69 nano-clay loading. Similarly, cellulose acetate (CA)/ Cu^{2+} MMt (3 % w/w clay) films
70 yielded high levels (>98 %) of inhibitory action against *Escherichia coli* ATCC 25922
71 (Bruna et al. 2014), whereas poly(lactic acid) (PLA)/ Cu^{2+} MMt films (Bruna et al. 2015)
72 were effective at reducing up to 99 % of *Escherichia coli* ATCC 25922 and *Listeria*
73 *innocua* ATCC 33090, when 5 % w/w Cu^{2+} MMt was added to each matrix.

74 To the best of the author's knowledge, there are no studies dealing with the potential of
75 protein/ Cu^{2+} MMt nanocomposites used as active food contact materials. Amongst
76 proteins, gelatin (Ge) is a water-soluble animal protein, obtained from the hydrolysis of
77 bone-collagen or connective tissues. It can be found as abundant waste/by product in
78 slaughter houses, and poultry and fish industries at reasonable cost (Hernandez-Muñoz
79 et al. 2004). Gelatin can be taken as a biogenic alternative to active films for being
80 classified as a "Generally Recognized as Safe" (GRAS) substance in the food additive
81 list by the U.S. Food and Drug Administration (FDA); also due to its biodegradability,
82 excellent film-forming ability, high oxygen barrier and satisfactory mechanical
83 properties at low or intermediate relative humidity (Hernandez-Muñoz et al. 2004;
84 Martucci et al. 2012). Nonetheless, the limited water resistance and mechanical strength
85 of gelatin films in moist environments still pose a problem to their wide application. In
86 earlier studies, the authors successfully demonstrated that blending gelatin with sodium
87 montmorillonite (Na^+ MMt) could enhance barrier, mechanical and moisture resistance
88 properties of films (Martucci et al. 2007; Martucci & Ruseckaite 2010), while
89 preserving their eco-friendliness (Martucci & Ruseckaite 2009). The best results were
90 obtained from films amended with 5 % w/w of Na^+ MMt, presenting the highest tensile

91 strength and Young's modulus, and the lowest WVP and hydrophilic surface (Martucci
92 & Ruseckaite 2010). This work presents the synthesis and characterization of Cu²⁺MMt
93 by acid-activated MMt through ion-exchange procedure, and the effect of incorporating
94 5 % w/w of modified clay on the physical properties and antimicrobial potential of
95 nanocomposite gelatin films against *E. coli* and *L. monocytogenes*, as a model of the
96 pathogens commonly found in foodstuffs.

97

98 2. EXPERIMENTAL SECTION

99 2.1. Chemicals and source of bacteria

100 Bovine hide gelatin (Ge) type B (Bloom strength 150, isoionic point (Ip) 5.3) was
101 kindly supplied by Rousselot (Buenos Aires, Argentina) and used with no further
102 treatment. Sodium montmorillonite (named as Na⁺MMt) was obtained from Southern
103 Clay Products Inc. (Texas, USA) under the trade name Cloisite Na⁺. The cation-
104 exchange capacity (CEC) was 92.6 meq/100 g of clay and the interlayer distance was
105 1.17 nm (as it was determined by X-ray diffraction on dry powder). Glycerol (Gly, 98
106 % reagent grade) and cupric sulphate pentahydrated (CuSO₄.5H₂O, 99.99 % purity)
107 were purchased from DEM (Mar del Plata, Argentina) and Anedra (Buenos Aires,
108 Argentina), respectively. All the other chemicals used were of analytical grade and
109 brought from Aldrich (St. Louis, MO, USA). Food-borne pathogens were selected to
110 assess the antibacterial properties: *Escherichia coli* O157:H7 ATCC 32158 (ATCC,
111 American Type Culture Collection) and *Listeria monocytogenes* ATCC 25923. Both
112 strains were plated onto eosin-methylene blue agar (EMB) and Baird Parker agar,
113 respectively (Martucci et al. 2015). The vegetative cells of each microorganism were
114 streaked on Mueller Hinton agar and incubated at 37 ± 0.5 °C for 24 h. Microbial broth
115 was then suspended in double distilled sterile water. The density of bacteria suspension

116 was adjusted until the visible turbidity was equal to 0.5 Mc Farland standards before
117 testing.

118 **2.2. Preparation of modified MMt**

119 Cu^{2+} MMt was obtained from acid-activated MMt (H^+ MMt) by ion exchange according
120 to the procedure described by Hu & Xia (2006) with minor modifications. H^+ MMt was
121 produced by suspending 10 g of Na^+ MMt in 75 mL of 0.05 M HCl solution. This
122 dispersion was kept for 24 h under constant stirring (400 rpm) at room temperature in a
123 hot plate (Cole Palmer, USA) and then centrifuged (Sartorius type4-15, Germany) at
124 5000 rpm for 5 min. The recovered sediment was washed with bi-distilled water until no
125 acid in the supernatant was detected, and then dried at 80 °C overnight in an air-
126 circulating oven (Mettler UFE550, Germany). The dry product was pulverized to an
127 average size of less than 300 mesh sieve. Cu^{2+} MMt was produced by dispersing 5 g of
128 dry H^+ MMt in 100 mL of a 0.05 M $\text{CuSO}_4 \cdot 5\text{H}_2\text{O}$ solution under gentle stirring (400
129 rpm) at 60 °C for 6 h. Afterwards the sample was submitted to the same purification
130 protocol than its acid-activated counterpart.

131 **2.3. Film forming process**

132 Gelatin films added with clay (i.e., Na^+ MMt, H^+ MMt and Cu^{2+} MMt; 5 % w/w dry
133 gelatin basis) and plasticized with glycerol (30 % w/w dry gelatin basis) were prepared
134 by the solution–intercalation method based on early works by the group (Martucci et al.
135 2007; Martucci & Ruseckaite 2009, 2010). Plasticizer and clay contents were fixed on
136 the basis of previous studies (Martucci & Ruseckaite 2008, 2010). Formulations with
137 glycerol content lower than 30 % w/w resulted in films behaving similarly to their un-
138 plasticized counterparts, while the incorporation of a glycerol level higher than 30 %
139 w/w induced plasticizer segregation and migration (Martucci & Ruseckaite 2008). In the
140 case of clay, gelatin nanocomposites containing 5 % w/w of Na^+ MMt displayed the best

141 set of thermal, mechanical, barrier and optical properties (Martucci & Ruseckaite 2008,
142 2010), so this percentage was selected for synthesis of the antibacterial nanocomposite
143 films. All films were preconditioned at 25 ± 2 °C and 65 ± 2 % RH for 48 h in an
144 environmental chamber before further experimental analysis. Films were designated as
145 Ge/Na⁺MMt, Ge/H⁺MMt and Ge/Cu²⁺MMt, respectively, depending on the clay used.

146 **2.4. Characterization**

147 **2.4.1. X-ray diffraction (XRD).** XRD patterns were recorded at room temperature on a
148 PANalytical X'Pert Pro diffractometer (Almelo, The Netherlands) equipped with a Cu
149 K α radiation source ($\lambda = 0.1546$ nm) at a generator voltage of 45 kV and 30 mA as the
150 applied current. The incidence angle ranged from 5° to 50° at a scanning rate of 1 °/min.
151 The interlayer spaces were calculated by the Bragg equation.

152 **2.4.2. Fourier Transform Infrared Spectroscopy (FTIR).** FTIR analyses were
153 performed on a Mattson Genesis II spectrophotometer in transmission mode. The
154 measurements were recorded between 4000–400 cm⁻¹ at 32 scans. Pulverized specimens
155 were pressed into pellets with KBr. The background noise was corrected with pure KBr
156 data.

157 **2.4.3. Energy dispersive X-ray spectroscopy (EDX).** EDX was used to assess the
158 presence of copper in MMT samples by using a spectrometer EMAX (Horiba Co. Ltd.,
159 Wycombe, U.K.) operated at $V_{acc} \frac{1}{4} 15$ kV.

160 **2.4.4. Thickness.** Film thickness was measured by a hand-held micrometer (Dial
161 Thickness gauge 7301, Mitutoyo Corporation, Kanagawa, Japan) with an accuracy of
162 0.01 mm. Measurements were taken at ten random locations from three films of each
163 formulation, and the mean thickness values were used to calculate the physical
164 properties.

165 **2.4.5. Visible light–barrier properties.** The light absorption of nanocomposite films
166 was measured in a wavelength ranging from 400 to 800 nm, using a UV-visible
167 spectrophotometer Shimadzu 1601 PC (Tokyo, Japan) according to a method described
168 elsewhere (Irissin-Mangata et al. 2001). Each film specimen was cut in rectangular
169 strips and placed directly in the spectrophotometer test cell. Air was used as reference.
170 Film opacity was expressed as the area under the absorption curve (arbitrary units/nm)
171 per thickness unit (mm). Reported values are the average of five measurements.

172 **2.4.6. Equilibrium moisture content (MC).** The squared-shape strips of each film
173 sample (dimensions 4 cm²) were weighed in an analytical balance (± 0.0001 g; Ohaus,
174 USA) to determine the initial mass. Then samples were dried in an air circulating oven
175 (Mettler, Germany) at 105 °C for 24 h according to the procedure reported in the
176 ASTM D644-94, 1994. The equilibrium moisture content (MC) was expressed as the
177 percentage of initial film weight lost during drying. Reported values are the average of
178 three replicates.

179 **2.4.7. Water vapor permeability (WVP).** Water vapor permeability (WVP) was
180 performed gravimetrically at 25 °C, following the ASTM E96-95 desiccant method. All
181 specimens were equilibrated at 65 ± 2 % RH at 25 ± 2 °C for 48 h. Afterwards, test
182 films were fixed onto opening cells containing silica gel (0 % RH), and the cells were
183 placed in a controlled humidity chamber at 65 ± 2 % RH and 25 ± 2 °C. The air gap
184 inside the cell was ~ 1.2 cm and the film area exposed for water vapor transmission was
185 13.8 cm². The cells were weighed on an hourly basis over a 10 h period. WVP was
186 calculated from the following equation:

$$187 \quad WVP(Kg \cdot m \cdot s^{-1} \cdot Pa^{-1} \cdot m^{-2}) = \frac{w}{At\Delta P} e \quad (1)$$

188 where w is the weight gain of the cup (Kg) at time t (s); e is the film thickness (m); A is
189 the film exposed area (m^2); ΔP is the vapor pressure difference across the film (Pa). All
190 measurements were taken in quadruplicate.

191 **2.4.8. Tensile properties.** The tensile strength (TS) and percentage of elongation at
192 break ($\epsilon\%$) were measured according to the ASTM 638 94 D standard using an Instron
193 4467 Universal Testing Machine (Buckinghamshire, England) with a 5 kN load cell at a
194 crosshead speed of 10 mm/min. Reported results were obtained from at least 10 samples
195 for each type of film

196 **2.4.9. Testing of antimicrobial activity.** The *in vitro* antibacterial activity of films and
197 clays was assessed following our previous work (Martucci et al. 2015) using agar disc-
198 diffusion assay. Test bacteria (100 μ L of inoculums containing approximately 10^5 - 10^6
199 CFU/mL of each bacterium) were plated onto Mueller Hinton (Merck, Darmstadt,
200 Germany) agar medium. Discs (10 mm in diameter) were cut from the films with a
201 circular knife and placed onto the inoculated plates. The antimicrobial activity of clay
202 specimens was assessed in a similar way. Each clay (3 mg), was dispersed in 1 mL of
203 bi-distilled water and submitted to an ultrasonic bath (Testlab, 160 W, 40 KHz) for 20
204 min. Then 30 μ L of the obtained suspension was poured into agar wells (5 mm
205 diameter). All plates were incubated at 37 °C for 24 h. The diameter of the inhibition
206 zone surrounding the film discs or wells (in the case of clays) was measured with a
207 manual caliper (Mitutoyo, Japan) from the center of the film. The antimicrobial activity
208 of clay specimens was assessed in a similar way. The result was determined as the mean
209 of three separate experimental runs.

210 **2.4.10. Cu²⁺ ion desorption studies.** Cu²⁺MMt (0.1 g) was extensively washed with bi-
211 distilled water under stirring for 24 h. The resulting dispersion was centrifuged at 8000
212 rpm (Sartorius type4-15, Germany) for 10 min. The concentration of the cupric cation

213 left in the washed Cu^{2+} MMt was determined by EDX. The *in vitro* antibacterial activity
214 of the washed clay was qualitatively measured with the agar disc-diffusion method, as
215 previously described for clays.

216 2.5. Statistical analysis

217 Experimental data were statistically analyzed by the one-way analysis of variance
218 (ANOVA) using the Origin Pro 8 software and Turkey's test for comparison of means at
219 a 5 % significance level. All the results are expressed as the mean \pm standard deviation.

220

221 3. RESULTS AND DISCUSSION

222 3.1. Modified clay characterization

223 X-ray diffraction patterns of pristine and modified clay were used to determine the
224 variations in the basal d_{001} -spacing due to cation switching (Figure 1). Na^+ MMt
225 exhibited a diffraction peak at $2\theta = 7.3^\circ$ (1.21 nm, according to Bragg eq.)
226 corresponding to the basal interlayer d_{001} -spacing (Mosser et al. 1997). Upon acid
227 activation, this reflection slightly shifted to lower angles corresponding to an interlayer
228 distance of 1.25 nm (Figure 1), in line with the exchange of Na^+ for H^+ with larger ionic
229 radius (ca. H^+ hydrated: 0.900 nm vs. Na^+ hydrated: 0.450 nm). The slight difference in
230 the basal reflection of montmorillonite caused by switching Na^+ for H^+ (Figure 1),
231 suggests that acid activation had a minor effect on the layered structure (Zhao et al.
232 2013). After treating H^+ MMt with CuSO_4 , the d_{001} -spacing increased up to 1.30 nm
233 (corresponding to $2\theta = 6.8^\circ$) confirming the intercalation of Cu^{2+} . The small increment
234 can be ascribed to the disparity between the ionic radius of the hydrated forms of Cu^{2+}
235 (i.e., hexaaqua) and Na^+ cations (He et al. 2001; Tanaka et al. 2007). A small new
236 reflection also appeared at around $2\theta = 13^\circ$ in the diffraction patterns of Cu^{2+} MMt,
237 probably attributed to an amorphous cupric hydroxide such as $\text{Cu}(\text{OH})_2 \cdot \text{H}_2\text{O}$, as already

238 accounted for by others (Zhou et al. 2004). The increment in *d*-spacing of MMt due to
239 Cu^{2+} ion exchange was previously observed, but values might vary due to differences in
240 the composition of the raw clay and the treatment performed on it (Zhou et al. 2004; Hu
241 & Xia 2006; Tanaka et al. 2007; Bruna et al. 2012, 2014, 2015).

242 EDX data further supported the presence of Cu^{2+} ions in the clay (Figure 2 c). Na^+ MMT
243 was distinguished by the presence of a peak at 0.05 eV in EDX spectrum assigned to
244 Na^+ which was absent in H^+ MMt and Cu^{2+} MMt spectra (Figures 2 a, b and c,
245 respectively). The occurrence of a new peak at 8 eV in Cu^{2+} MMt spectrum (Figure 2 c)
246 is a strong experimental evidence of copper exchange (Bagchi et al. 2013; Das et al.
247 2013). Since the intensity of such peak is proportional to the element concentration, the
248 loading of Cu^{2+} cation onto MMt was estimated in about 3 % (on element basis) (Figure
249 2 c).

250 The effect of the cation exchange on the clay structure was analyzed by FTIR (Figure
251 3). All the spectra exhibited relevant absorption bands at 3631 cm^{-1} (stretching vibration
252 of structural OH group (Al-OH)), 3432 and 1631 cm^{-1} (stretching and bending
253 vibrations of interlayer H_2O , respectively), 1045 cm^{-1} (stretching vibration of Si-O), and
254 $915\text{-}18\text{ cm}^{-1}$ (Al-Al-OH bending vibration) characteristic of clay structure (Zhou et al.
255 2004; Zhao et al. 2013; Pereira et al. 2013). The absorption feature of Na^+ MMt
256 remained unchanged after acid activation, thereby suggesting that the aluminum cations
257 of montmorillonite seemed not to be leached by the acid treatment, as postulated by
258 others (Tong et al. 2005). The peak situated at 3631 cm^{-1} was slightly shifted
259 downwards upon Cu^{2+} exchange, which is explained by the presence of interactions
260 between cupric ions and clay, primarily in the inter-lamellar space, through
261 complexation of copper ions as previously indicated by other authors (Bagchi et al.
262 2013; Pereira et al. 2013). The intensity of the hydration band barely changed due to

263 differences in the water coordination capacity of Na^+ and Cu^{2+} ions. Finally other
264 characteristic vibrations of the tetrahedral sheets, namely Si-O-Si stretching (993 cm^{-1})
265 and Si-O-Al bending (521 cm^{-1}), reached higher wave length values and decreased
266 intensity indicating a somewhat disordered MMt structure (Xia et al. 2010).

267 The inhibitory activity of pristine and modified clay against Gram-negative and Gram-
268 positive bacteria was investigated with the agar disc diffusion method, and results are
269 summarized in Table 1. Both pathogens revealed sensitivity to all clay suspensions,
270 indicating certain Na^+ MMt antibacterial activity. The ability of Na^+ MMt, Ca^{2+} MMt and
271 H^+ MMt to reduce the bacterial plate counts of *E. coli* was previously observed by Hu &
272 Xia (2006), though no reports on the inhibitory effect on Gram-positive bacteria have
273 come to light. Cu^{2+} MMt, on the other hand, exerted a powerful antibacterial action
274 against both bacteria tested ($p < 0.05$), related to the higher adsorption capacity of this
275 clay (Guo et al. 2011) and the intrinsic antibacterial activity of Cu^{+2} (He et al. 2001; Hu
276 and Xia 2006; Malachová et al. 2011). The presence of Cu^{2+} cations leads to a surplus
277 of positive charge onto the mineral surface. They serve as potential attachment sites for
278 negatively charged cell surface (Stotzky 1980), and result in the appearance of defects
279 in the bacterial outer membrane responsible for the cell permeability, so that cell
280 contents are lost. The higher susceptibility of *L. monocytogenes* to Cu^{2+} MMt (Table 1)
281 could be related to differences in the composition and thickness of the outer membrane
282 of Gram-positive and Gram-negative bacteria (Hu et al. 2005; Malachová et al. 2009).
283 The cell wall of Gram-positive bacteria is thicker than that of Gram-negative bacteria
284 due to the presence of a thick peptidoglycan layer (20-80 nm) containing phosphate and
285 carboxylic groups. This layer provides a negatively charged site onto the cell wall of
286 Gram-positive bacteria where cations bind. Gram-negative bacteria have a thinner
287 monolayer of peptidoglycan, lipopolysaccharide and phospholipids, phospholipids being

288 the only main binding site for cations (Vaara 1992). Such differences in the cell wall
289 structures of Gram-positive and Gram-negative bacteria turned *L. monocytogenes* more
290 vulnerable to Cu^{2+} MMt.

291 Cu^{2+} MMt slightly reduced its antibacterial activity (about 10 % of the original, Table 1)
292 after extensive washing for 24 h, evidencing that copper is retained onto the clay surface
293 (Hu et al. 2005; Hu & Xia 2006). EDX results also confirmed the high retention rate of
294 copper after washing, copper desorption being below 8 % (data not shown).

295 **3.2. Characterization and comparison of the functional properties of control** 296 **and Ge/ Cu^{2+} MMt films**

297 **3.2.1. Structural analysis**

298 The diffractogram of the unfilled gelatin film (control) displayed a broad and low
299 intensity peak at $2\theta = 6.2\text{-}9.5^\circ$ representing the typical amorphous state of gelatin films
300 produced at a temperature higher than the helix-coil transition ($T_{\text{helix-coil}} \sim 35^\circ\text{C}$) (Figure
301 4) (Martucci et al. 2007). The XRD of the nanocomposite films was characterized by the
302 presence of shoulders at $2\theta < 7^\circ$ denoting a certain degree of matrix component
303 intercalation, i.e., gelatin and/or glycerol, into the clay galleries causing widening of the
304 *d*-space relative to that of the pristine MMt (Figure 4). (Martucci et al. 2007; Rao et al.
305 2007; Martucci & Ruseckaite 2010; Farahnaky et al. 2014; Nagarajan et al. 2014).

306 The FTIR spectra of un-filled Na^+ MMt and Cu^{2+} MMt- incorporated gelatin films
307 (Figure 5) presented characteristic peaks in the amide region at 1631 cm^{-1} (amide I,
308 C=O stretching), 1551 cm^{-1} (amide II, N-H bending,), and 1237 cm^{-1} (amide III, C-N
309 and N-H) (Sionkowska et al. 2004; Martucci & Ruseckaite 2010). The addition of clay
310 shifted amide-I, amide-II and amide-III to higher frequency c.a. 1646, 1553, and 1245
311 cm^{-1} , respectively, confirming the occurrence of hydrogen bonding interactions between
312 gelatin and acceptor atoms such as oxygen from free-OH and Si-O-Si groups in MMt,

313 as documented for other protein-MMt composites (Kumar et al. 2010; Martucci &
314 Ruseckaite 2010).

315 **3.2.2. Optical properties**

316 The neat gelatin film was transparent without any color tint, while nanocomposites were
317 less transparent and colored as Ge/Cu²⁺MMt. The light transmission capacity of gelatin
318 films was reduced by clay addition (Table 2, $p < 0.05$), indicating a strong light scattering
319 effect due to clay particles with sizes higher than the wave-length of the visible light
320 (Martucci & Ruseckaite 2010; Shotornivit et al. 2010; Rhim 2013). The sharp decrease
321 in transparency experienced by the Ge/Cu²⁺MMt film should be attributed not only to
322 the scattering explained by some clay structures but also to coloration increase due to
323 the transformation of some cupric ions to cupric oxides during the drying stage of the
324 film manufacturing process, as previously described by Bruna and co-workers (Bruna et
325 al. 2012). The significant differences noticed in the parameter analyzed were not
326 detected when the films' visual appearance was qualitatively observed, since all
327 specimens remained transparent.

328 **3.2.3. Moisture content, water vapor permeability and tensile properties**

329 The average moisture content (MC) of all films remained around 13.8 ± 1.6 g of
330 water/100 g of film (Table 2). The constancy of MC at any cation in MMt suggests that
331 the hydration capacity of cations did not affect the moisture uptake capacity of the
332 nanocomposite films.

333 The water vapor barrier property of gelatin films was substantially improved ($p < 0.05$,
334 Table 2) by adding 5 % w/w MMt regardless of the cation intercalated, suggesting that
335 switching the cation marginally alters the hydrophilic/hydrophobic balance of the filler.
336 The strong interactions between gelatin and nano-clays (Martucci & Ruseckaite 2010)
337 consume some hydrophilic groups, reducing the water uptake by capillarity at the

338 interface. The presence of water vapor impermeable silicate platelets or other structures
339 with large aspect ratios dispersed in the polymer matrix also contribute to obstructing
340 and delaying the transmission of water vapor through the matrix, as postulated for other
341 protein nanocomposite films (Farahnaky et al. 2014; Kanmani & Rhim 2014; Nagarajan
342 et al. 2014).

343 The incorporation of 5 % w/w MMt noticeably improved ($p < 0.05$) TS values as
344 compared to control. The great affinity of biopolymer and nano-clay limiting the
345 molecular mobility of protein chains, together with the uniform dispersion of the nano-
346 reinforcements might lead to an increase in TS (Martucci & Ruseckaite 2010;
347 Farahnaky et al. 2014; Nagarajan et al. 2014). The differences in tensile strength
348 between our nanocomposites and other reported in the literature could be attributed to
349 differences in clay type, matrix source, processing technologies, or a combination
350 thereof. The extensibility decreased significantly ($p < 0.05$) in about 42 % when adding 5
351 % w/w clay, and no major effects ($p > 0.05$) were detected with cation exchange in MMt
352 (Table 2). The reduction in $\epsilon\%$ was previously reported in gelatin-based
353 nanocomposites (Rao et al. 2007; Martucci & Ruseckaite 2010; Kanmani & Rhim 2014;
354 Farahnaky et al. 2014), and has been attributed to the restricted motion of gelatin
355 molecules due to interfacial interactions between gelatin and nano-clay.

356 **3.2.4. Antimicrobial activity**

357 Antibacterial assays (Table 3) indicate that free-MMt gelatin films have shown little
358 antimicrobial activity against both Gram-negative and Gram-positive pathogenic
359 bacteria, probably due to the presence of short chain polypeptides (Minervini et al 2003;
360 Di Bernardini et al. 2010). Clay addition enlarged the diameter of the clearing zone
361 (Table 3) and the activity visibly varied with the cation in MMt and the pathogen tested.
362 The Ge/Cu²⁺MMt film exhibited the highest inhibitory activity, in agreement with the

363 antimicrobial performance of clays (Table 1). Overall, Ge/Cu²⁺MMt film greatly
364 inhibited the growth of Gram-positive (*L. monocytogenes*) as compared to Gram-
365 negative (*E. coli*) pathogens (Table 3). The inhibitory action of Ge/Cu²⁺MMt against
366 both microorganisms was assumed to be similar to that described above for Cu²⁺MMt:
367 attachment to clay surface, followed by cell wall damage, loss of cell content and,
368 eventually microbial death (Hu et al. 2005; Guo et al. 2011). These results are consistent
369 with the reduction of 98 % of *E. coli* colonies exposed to cellulose acetate films
370 incorporated with 5 % w/w of Cu²⁺MMt (Bruna et al. 2014) and 99 % of *Escherichia*
371 *coli* ATCC 25922 and *Listeria innocua* ATCC 33090 colonies in contact with PLA/5 %
372 w/w Cu²⁺MMt (Bruna et al. 2015).

373

374 4. CONCLUSION

375 This manuscript shows the feasibility of preparing antibacterial Ge/Cu²⁺MMt films with
376 extended time of action by immobilizing Cu²⁺ through complexation with hydroxyl
377 groups in montmorillonite. Cu²⁺MMt demonstrated low leaching level in the tested
378 conditions and retained about 90 % of its inhibitory activity against *E. coli* and *L.*
379 *monocytogenes*. Yet its sensitivity varied with the ability of the tested bacteria to attach
380 to the positively charged clay surface. The addition of Cu²⁺MMt as inorganic
381 antibacterial into the gelatin matrix enhanced several key properties for packaging
382 applications (tensile strength increased 280 %, and water vapor permeability declined
383 43 %) and sufficed to inhibit Gram negative and Gram positive bacteria at relatively low
384 loading growth (c.a. 5 % w/w Cu²⁺MMt). Studies on the evaluation of copper ions
385 release from nanocomposite films exposed to food simulants are being conducted in
386 order gain insight into the potential risk assessment of their use as food contact
387 materials.

388

389 **5. REFERENCES**

- 390 Bagchi, B., Kar, S., Dey, S., Bhandary, S., Roy, D., Mukhopadhyay, T., Das, S., &
391 Nandy, P. (2013). In situ synthesis and antibacterial activity of copper nanoparticle
392 loaded natural montmorillonite clay based on contact inhibition and ion release.
393 *Colloids and Surfaces B: Biointerfaces* 108, 358–365
- 394 Bruna, J. E., Galotto, M. J., Guarda, A., & Rodriguez, F. (2014). A novel polymer based
395 on MtCu²⁺/cellulose acetate with antimicrobial activity. *Carbohydrate Polymers* 102,
396 317-323
- 397 Bruna, J. E., Peñaloza, A., Guarda, A., Rodríguez, F., & Galotto, M. J. (2012).
398 Development of MtCu²⁺/LDPE nanocomposites with antimicrobial activity for
399 potential use in food packaging. *Applied Clay Science* 58, 79–87
- 400 Bruna, J. E., Quilodrán, H., Guarda, A., Rodríguez, F., Galotto, M. J., & Figueroa, P.
401 (2015). Development of antibacterial MtCu/PLA nanocomposites by casting method for
402 potential use in food packaging *Journal of the Chilean Chemical Society* 60, 2868-2873
- 403 Das, D., Nath, B. C., Phukon, P., & Dolui, S. K. (2013). Synthesis and evaluation of
404 antioxidant and antibacterial behavior of CuO nanoparticles. *Colloids and Surfaces B:*
405 *Biointerfaces* 101, 430-433
- 406 Di Bernardini, R., Harnedy, P., Bolton, D., Kerry, J., O'Neill, E., Mullen, A. M. (2011)
407 Antioxidant and antimicrobial peptidic hydrolysates from muscle protein sources and
408 by-products. *Food Chemistry* 124, 1296-1307
- 409 Drelich, J., Li, B., Bowen, P., Hwang, J-Y, Mills, O., & Hoffman, D. (2011).
410 Vermiculite decorated with copper nanoparticles: novel antibacterial hybrid material.
411 *Applied Surface Science* 257, 9435–9443



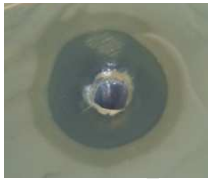
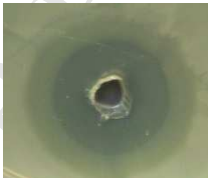


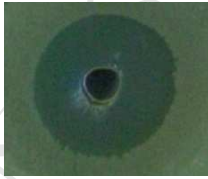
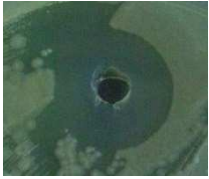
- 412 Farahnaky, M., Dadfar, S. M. M., & Shahbazi, M. (2014). Physical and mechanical
413 properties of gelatin–clay nanocomposite. *Journal of Food Engineering* 122, 78–83
- 414 Guo, Z., Li, Y., Zhang, S., Niu, H., Chen, Z., & Xu, J. (2011). Enhanced sorption of
415 radiocobalt from water by Bi (III) modified montmorillonite: a novel adsorbent. *Journal*
416 *of Hazardous Materials* 192, 168–175
- 417 He, H. P., Guo, J. G., Xie, X. D., & Peng, J. L. (2001). Location and migration of
418 cations in Cu²⁺-adsorbed montmorillonite. *Environment International* 26 (5–6), 347–
419 352
- 420 Hernandez-Muñoz, P., Villalobos, R., & Chiralt, A. (2004). Effect of cross-linking
421 using aldehydes on properties of glutenin rich films. *Food Hydrocolloid* 18, 403-411
- 422 Hu, C-H., & Xia, M-S. (2006). Adsorption and antibacterial effect of copper-exchanged
423 montmorillonite on *Escherichia coli* K88. *Applied Clay Science* 31 (2006) 180–184
- 424 Hu, C-H., Xu, Z-R., & Xia, M-S. (2005). Antibacterial effect of Cu²⁺-exchanged
425 montmorillonite on *Aeromonas hydrophila* and discussion on its mechanism *Veterinary*
426 *Microbiology* 109, 83–88
- 427 Irissin-Mangata, J., Bauduin, G., Boutevin, B., & Gontard, N. (2001). New plasticizers
428 for wheat gluten films. *European Polymer Journal* 37, 1533-1541
- 429 Kanmani, P., & Rhim, J-W. (2014). Physical Mechanical and Antimicrobial Properties
430 of Gelatin Based Active Nanocomposite Films Containing AgNPs and Nanoclay. *Food*
431 *Hydrocolloids* 35, 644–652
- 432 Klopogge, J. T., Mahmutagic, E., & Frost, R. L. (2006). Mid Infrared and Infrared
433 Emission Spectroscopy of Cu-Exchanged Montmorillonite. *Journal of Colloid and*
434 *Interface Science* 296(2), 640-646

- 435 Kumar, P., Sandeep, K. P., Alavi, S., Truong, V. D., & Gorga, R. E. (2010). Preparation
436 and characterization of bio-nanocomposite films based on soy protein isolate and
437 montmorillonite using melt extrusion. *Journal of Food Engineering* 100(3), 480-489
- 438 Llorens, A., Lloret, E., Picouet, P. A., Trbojevich, R., & Fernandez, A. (2012). Metallic-
439 based micro and nanocomposites in food contact materials and active food packaging
440 *Trends in Food Science & Technology* 24, 19-29
- 441 Malachová, K., Praus, P., Pavlíčková, Z., & Turicová, M. (2009). Activity of
442 antibacterial compounds immobilised on montmorillonite. *Applied Clay Science* 43,
443 364–368
- 444 Malachová, K., Praus, P., Rybková, Z., & Kozák, O. (2011). Antibacterial and
445 antifungal activities of silver, copper and zinc montmorillonites. *Applied Clay Science*
446 53, 642–645
- 447 Martucci, J. F., & Ruseckaite, R. A. (2010). Biodegradable Bovine Gelatin/Na+-
448 Montmorillonite Nanocomposite Films. Structure, Barrier and Dynamic Mechanical
449 Properties. *Polymer-Plastics Technology and Engineering* 49(6), 581-588
- 450 Martucci, J. F., & Ruseckaite, R. A. (2009). Biodegradation of three-layer laminate
451 films based on gelatin under indoor soil conditions. *Polymer Degradation and Stability*
452 94, 1307–1313
- 453 Martucci, J.F., & Ruseckaite, R.A. (2008). Structure and properties of
454 gelatine/montmorillonite nanocomposite films, in *Recent Advances in Research on*
455 *Biodegradable Polymers and Sustainable Polymers. Volume 1*, A. Jimenez, G.E. Zaikov
456 (Eds), Nova Publishers, Huntington, NY, pp. 27-36. ISBN 978-1-60692-095-4
- 457 Martucci, J.F., Accareddu, A.M.E., & Ruseckaite, R.A. (2012). Preparation and
458 Characterization of Plasticized Gelatin Films Cross-Linked With Low Concentrations of
459 Glutaraldehyde. *Journal of Material Science* 47(7), 3282-3292

- 460 Martucci, J. F., Gende, L. B., Neira, L. M., & Ruseckaite, R. A. (2015). Oregano and
461 lavender essential oils as antioxidant and antimicrobial additives of biogenic gelatin
462 films. *Industrial Crops and Products* 71, 205–213
- 463 Martucci, J. F., Vázquez, A., & Ruseckaite, R. A. (2007). Nanocomposites based on
464 gelatin and montmorillonite. Morphological and thermal studies. *Journal of Thermal*
465 *Analysis and Calorimetry* 89(1), 117-122
- 466 Minervini, F., Algaron, F., Rizzello, C. G., Fox, P. F., Monnet, V., & Gobbetti, M.
467 (2003). Angiotensin I-converting-enzyme-inhibitory and antibacterial peptides from
468 *Lactobacillus helveticus* PR4 proteinase-hydrolysed casein of milk from six species.
469 *Applied and Environmental Microbiology* 69, 5297-5305
- 470 Mosser, C., Michot, L. J., Villiers, F., & Romeo, M. (1997). Migration of cations in
471 Cu(II)-exchanged montmorillonite and laponite upon heating. *Clays and Clay Minerals*
472 45, 789–802
- 473 Nagarajan, M., Benjakul, S., Prodpran, T., & Songtipya, P. (2014). Characteristics of
474 bio-nanocomposite films from tilapia skin gelatin incorporated with hydrophilic and
475 hydrophobic nanoclays *Journal of Food Engineering* 143, 195-204
- 476 Pereira, F. A. R., Sousa, K. S., Cavalcanti, G. R. S., Fonseca, M. G., de Souza, A. G., &
477 Alves, A. P. M. (2013). Chitosan-montmorillonite biocomposite as an adsorbent for
478 copper (II) cations from aqueous solutions. *International Journal of Biological*
479 *Macromolecules* 61, 471–478
- 480 Rao, Y. (2007). Gelatin-clay nanocomposites of improved properties. *Polymer* 58(18),
481 5369-5375
- 482 Rhim, J-W., Park, H-M., & Ha, C-S. (2013). Bio-nanocomposites for food packaging
483 applications. *Progress in Polymer Science* 38(10-11), 1629–1652

- 484 Sionkowska, A., Wisniewski, M., Skopinska, J., Kennedy, C. J., & Wess, T. J. (2004).
485 Molecular interactions in collagen and chitosan blends. *Biomaterials* 25, 795–801
- 486 Stotzky, G. (1980) Surface interactions between clay minerals and microbes, viruses,
487 and soluble organics, and the probable importance of these interactions to the ecology
488 of microbes in soil. In *Microbial Adhesion to Surfaces* (eds. R. C. BERKELEY et al.),
489 pp. 233-247. Soc. Chem. Industry, London.
- 490 Tanaka, M., Itadani, A., Abe, T., Taguchi, H., & Nagao, M. (2007). Observation of
491 characteristic IR band assignable to dimerized copper ions in montmorillonite. *Journal*
492 *of Colloid and Interface Science* 308, 285–288
- 493 Tong, G., Yulongo, M., Peng, G., & Zirong, X. (2005). Antibacterial effects of the
494 Cu(II)-exchanged montmorillonite on *Escherichia coli* K88 and *Salmonella*
495 *choleraesuis*. *Veterinary Microbiology* 105(2), 113–122
- 496 Vaara M. (1992). Agents that increase the permeability of the outer membrane.
497 *Microbiology and Molecular Biology Reviews* 56, 3395-3411.
- 498 Xia, M., Jiang, Y., Zhao, L., Li, F., Xue, B., Sun, M., Liu, D., & Zhang, X. (2010). Wet
499 grinding of montmorillonite and its effect on the properties of mesoporous
500 montmorillonite *Colloids and Surfaces A: Physicochemical and Engineering Aspects*
501 356, 1–9
- 502 Zhao, H., Zhou, C. H., Wu, L. M., Lou, J. Y., Li, N., Yang, H. M., Tong, D. S., & Yu,
503 W. H. (2013). Catalytic dehydration of glycerol to acrolein over sulfuric acid-activated
504 montmorillonite catalysts. *Applied Clay Science* 74, 154–162
- 505 Zhou, Y. H., Xia, M. S., Ye, Y., & Hu, C. H. (2004). Antimicrobial ability of Cu²⁺-
506 montmorillonite. *Applied Clay Science* 27 (3–4), 215–218.
- 507

Table 1. Antimicrobial activity against *E. coli* and *L. monocytogenes* of clays measured as inhibition zone.

d₀: 5mm	Inhibition zones (mm)			
	Na⁺MMt	H⁺MMt	Cu²⁺MMt	Cu²⁺MMt (after release)
<i>E. coli</i>	12.0±2.8 a 	12.5±2.1 a 	15.5±0.7 b 	14.0±1.0 b 
<i>L. monocytogenes</i>	11.0±1.4 a 	15.5±0.8 bc 	16.5±0.7 b 	14.5±0.5 c 

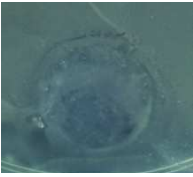


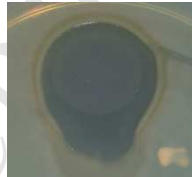




Any two means in the same row followed by the same letter are not significantly (P>0.05) different according to Turkey test.

Table 2. Thickness, opacity, Water vapor permeability (WVP), moisture content (MC), tensile strength (TS) and elongation at break ($\epsilon\%$) of obtained gelatin films.

	Thickness (mm)	Opacity (uA*nm)	WVP*10¹³ (Kg/Pa.s.m) RH 65:0	MC (%)	TS (MPa)	$\epsilon\%$ (%)
Ge	0.21±0.04 a	33.0±2.0 a	2.50±0.13 a	14.00±1.25 a	3.9±1.0 a	96.9±11.9 a
Ge/Na⁺MMt	0.15±0.02 a	49.0±3.0 b	1.62±0.14 b	13.74±0.62 a	11.9±1.6 b	56.4±6.8 b
Ge/H⁺MMt	0.18±0.06 a	51.0±9.0 b	2.04±0.30 b	13.78±0.58 a	9.9±1.6 b	49.8±6.9 b
Ge/Cu²⁺MMt	0.16±0.03 a	89.8±13.0 c	1.43±0.40 b	13.58±1.03 a	10.9±1.4 b	48.4±7.8 b

Any two means in the same column followed by the same letter are not significantly ($P>0.05$) different according to Turkey test.

Table 3. Antimicrobial activity against *E. coli* and *L. monocytogenes* measured as inhibition zone expressed as millimeter (mm) of Ge films with and without clays.

d₀:15mm	Inhibition zone (mm)			
	Ge	Ge/Na⁺MMt	Ge/H⁺MMt	Ge/Cu²⁺MMt
<i>E. coli</i>	15.0±0.0 a 	19.5±0.7 b 	24.0±1.4 c 	23.5±0.7 c 
<i>L. monocytogenes</i>	16.0±1.0 a 	30.5±0.7 b 	33.5±0.7 c 	37.0±2.8 c 

Any two means in the same row followed by the same letter are not significantly ($P>0.05$) different according to Turkey test.

1 **FIGURE CAPTIONS**

2 **Figure 1.** XRD pattern of Na⁺MMt (___), H⁺MMt (....) and Cu²⁺MMt (----).

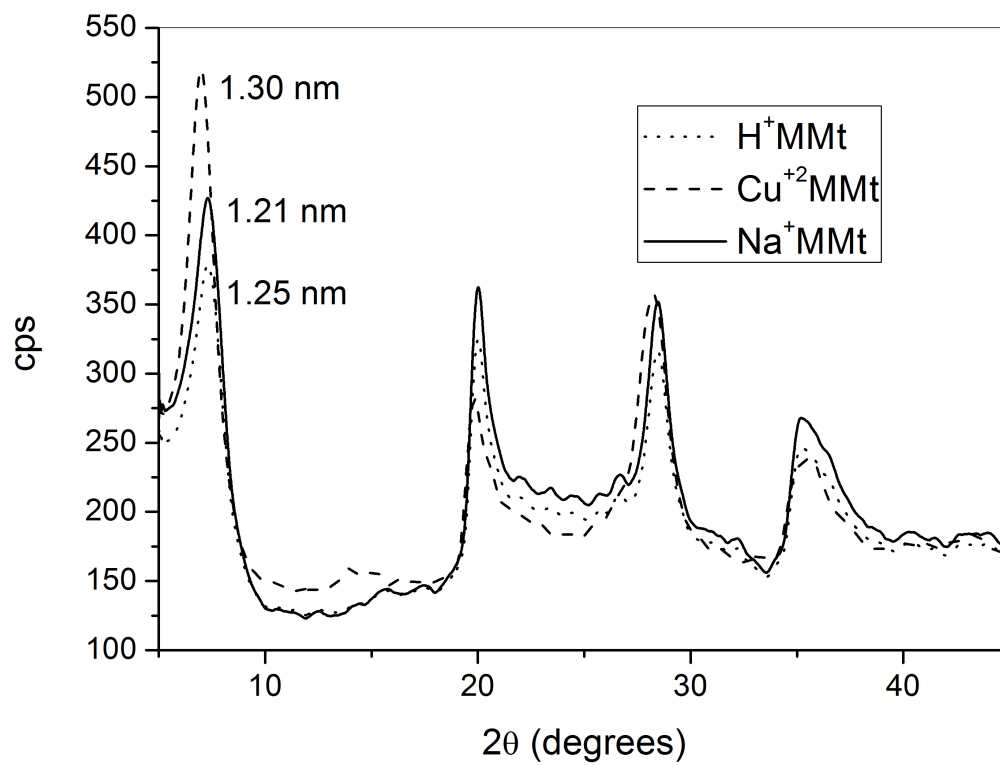
3 **Figure 2.** Chemical composition of a) Na⁺MMt, b) H⁺MMt and c) Cu²⁺MMt
4 determined by EDX.

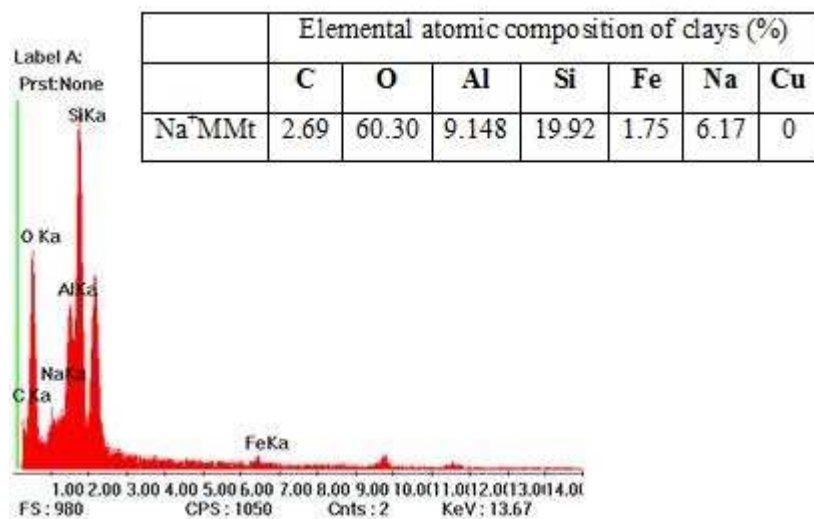
5 **Figure 3.** FTIR spectra between 4000–400 cm⁻¹ for Na⁺MMt(___), H⁺MMt (....) and
6 Cu²⁺MMt (----).

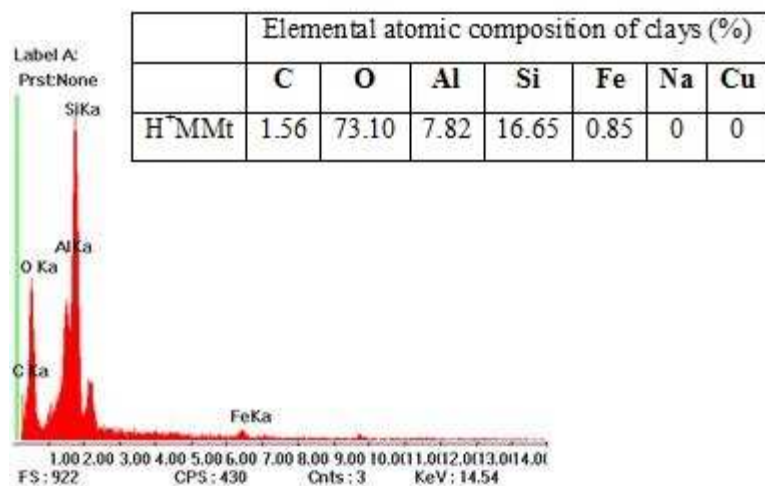
7 **Figure 4.** XRD pattern of Ge (-.-.-), Ge/Na⁺MMt (___), Ge/H⁺MMt (....) and
8 Ge/Cu²⁺MMt (----) films.

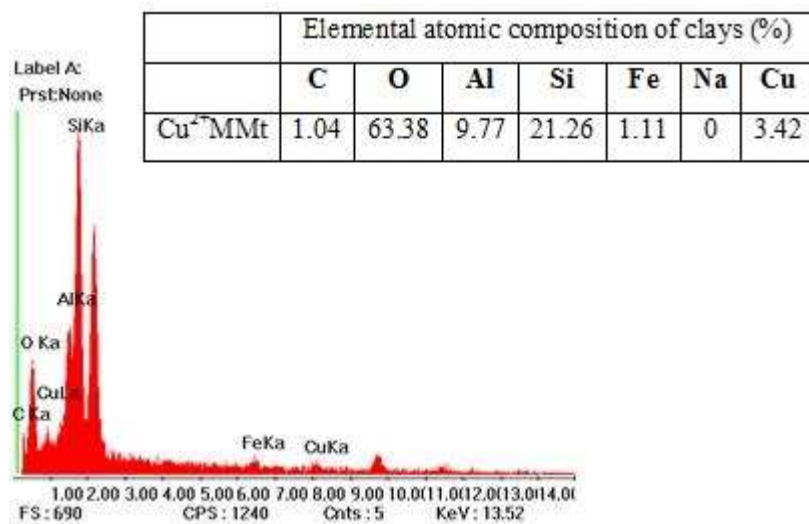
9 **Figure 5.** FTIR spectra of Ge (-.-.-), Ge/Na⁺MMt (___), Ge/H⁺MMt (....) and
10 Ge/Cu²⁺MMt (----) films.

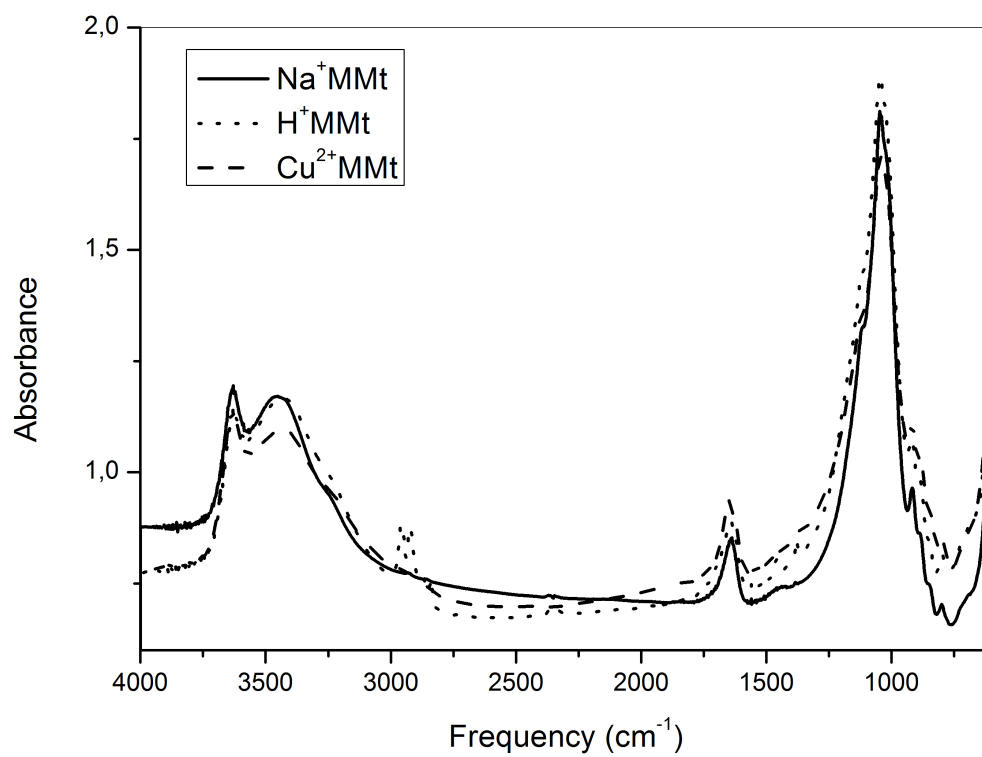
11

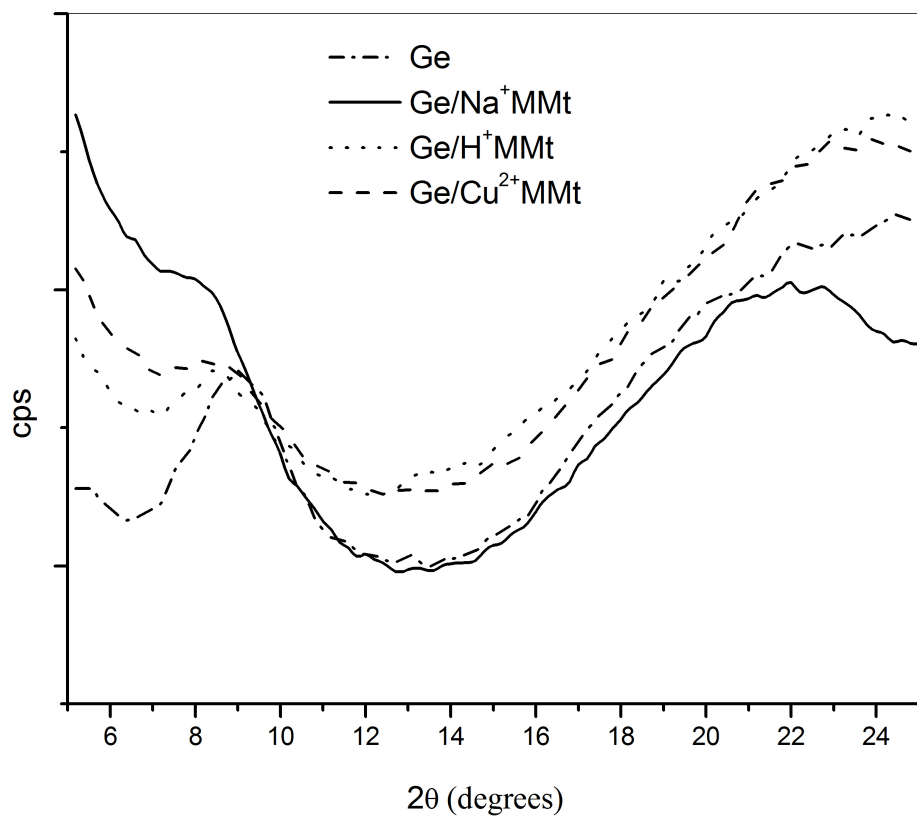




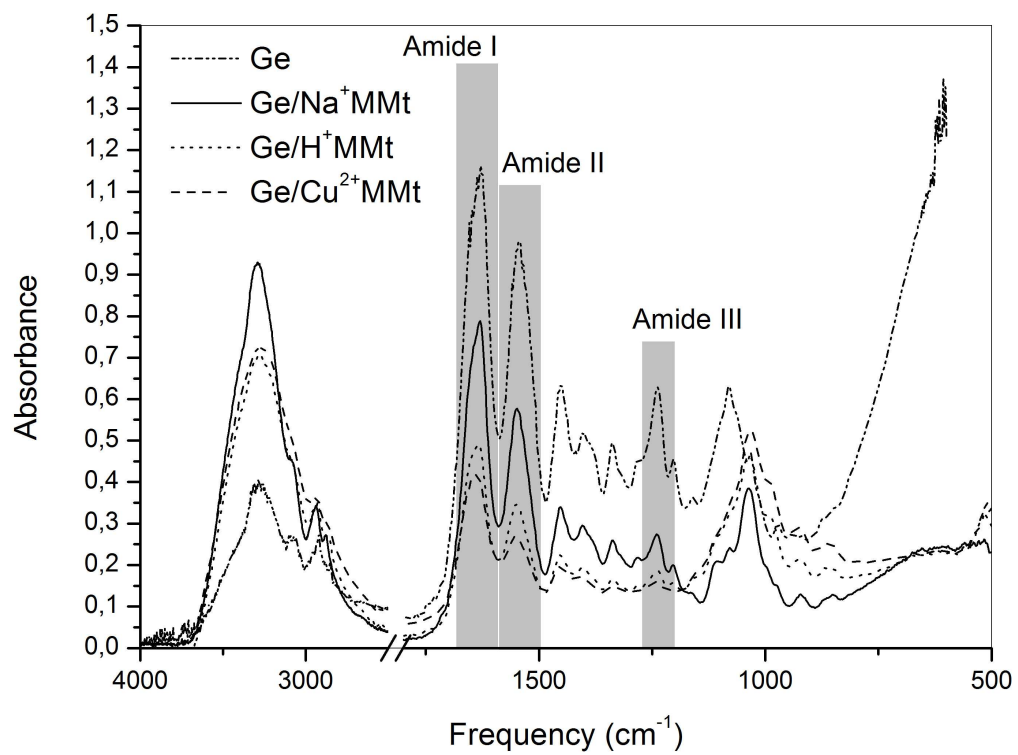








ACCEPTED



Highlights

1. Cu^{2+} MMt was obtained by ion exchange from acid activated Na^+ MMt
2. Cu^{2+} MMt showed strong activity against *E. coli* and *L. monocytogenes*
3. Inclusion of 5 % w/w clay enhanced tensile strength and water vapor barrier of gelatin films
4. Significant antibacterial property was observed for Ge/ Cu^{2+} MMt films